

Research Article

Simulation Research on the Performance of PEMEC with Single Channel Flow Field Established by Orthogonally Sinusoidal Function with Different Amplitudes and Angular Frequencies

Dehui Yang , Hongyu Wang , Yuanyuan Li , Menghan Liu , Jinyan Han ,
and Naibao Huang 

Transportation Engineering College, Dalian Maritime University, Dalian, Liaoning 106026, China

Correspondence should be addressed to Hongyu Wang; wanghongyusci@yeah.net

Received 23 October 2023; Revised 17 December 2023; Accepted 1 January 2024; Published 16 January 2024

Academic Editor: Denis Osinkin

Copyright © 2024 Dehui Yang et al. This is an open access article distributed under the Creative Commons Attribution License, which permits unrestricted use, distribution, and reproduction in any medium, provided the original work is properly cited.

As one of the main hydrogen production devices, the performance of the proton exchange membrane electrolytic cell (PEMEC) is directly related to the geometric design of the flow channel. In this paper, a new orthogonally sinusoidal channel with periodic fluctuations in both horizontal and vertical planes is proposed. The effects of amplitude and angular frequency in two orthogonally sinusoidal channels with the same or opposite frequency on PEMEC performance are studied by numerical simulation. The results show that the spatial amplitude and angular frequency effectively improve the electrochemical performance and mass transfer performance of PEMEC. Compared with Case 1-1, the polarization performance of Case 7-2 is increased by 16.39% because of the largest spatial amplitude. The oxygen content at 40 mm away from the inlet in the diffusion layer is also decreased by 42.63%. The horizontal angular frequency can increase the hydrogen content by 11.07% at most in Case 5-2. However, the increase in vertical angle frequency will inhibit the oxygen removal on the anode side. The sinusoidal flow channel in orthogonal spaces will provide a particular reference for the design of PEMEC in the future.

1. Introduction

In recent years, since fossil energy consumption makes the problem of energy shortage increasingly prominent [1, 2], hydrogen energy has begun to receive much attention as a representative of clean energy [3, 4]. Among many technologies for producing hydrogen as a stable carrier by converting [5–7] and storing excess electric energy [8, 9] by electrolysis of water, proton exchange membrane electrolysis cell (PEMEC) is considered a promising technology due to its advantages such as small volume of reaction device [10], high purity of hydrogen production [11], and strong adaptability [12]. However, the acidic environment in the PEMEC imposes more stringent requirements on the performance of key components such as proton exchange membranes, electrodes, and bipolar plates [13–15]. Among these components, the flow channel in the bipolar plate is the most critical structural element in the electrolytic cell [16, 17].

As a channel for transporting liquid water and discharging product gas, the geometric design of the flow channel determines the spatial distribution of materials [18, 19]. Gayen et al. [20] placed baffles at the inlet of the microchannel to obtain uniform material spatial distribution and heat transfer. This spatial distribution can be divided into two main kinds: one is in the horizontal plane and the other one is in the vertical plane. In recent decades, researchers have conducted a series of studies on these two main flow behaviors in channels.

The researchers first investigated the effects of periodicities and fluctuations on PEMEC performance in the vertical plane. The vertical fluctuations can not only maintain the electrolytic cell operating environment stable but also make the water transfer along the vertical plane with quick removal of produced bubbles by forced convection to improve the life and mass transfer capacity of PEMEC [21]. Since the geometric design of the vertical plane can

determine levels of forced convection, Bilgili et al. [22] also set periodic blocks in the vertical plane of the flow channel to cause forced convection. Khatib et al. [23] paid attention to the vertical planes and studied the influence of the fluctuant geometrical parameters in PEMEC with open-cell foam material on forced convection of the fluid. Therefore, the geometrical parameters of the fluctuations should be considered a critical factor in the design of the flow channel.

Besides the geometrical parameters of vertical fluctuations, the same vertically periodic structures were also investigated by Wang et al. [24] with raised periodic structures in an interdigitated flow channel. The presence of periodic structures in the flow channel has been observed to enhance the performance of PEMEC. Wang et al. [25] designed the flow channel with a periodic wave structure in the vertical direction. Compared with the conventional straight flow channel, the maximum power density of the periodic wave structure channel was increased by 4%. Tugirumubano et al. [26] discovered that an increased frequency resulted in more vertical liquid to flush and exhaust bubbles through the sinking periodic structure to improve electrolysis efficiency significantly. Though the necessity of periodic fluctuations in the vertical plane to the performance of PEMEC is proved in the above studies, the attention to these periodic fluctuations is only focused on the vertical plane. Due to the lack of horizontal planes, these studies on periodic fluctuations are insufficient.

Since the design of a horizontal structure also plays a crucial role in guiding fluid fluctuation in the horizontal plane, researchers further investigated the effects of periodicities and fluctuations on PEMEC performance in the horizontal plane. Toghyani et al. [27] found that compared with the parallel flow channel, the more extended serpentine flow channel with a number of corners exhibited horizontal fluctuations to increase current density and hydrogen production efficiency in PEMEC by promoting fluid rotation. In addition, Toghyani et al. [28] also further designed the channel with a spiral structure to enhance horizontal fluctuations. Zhou et al. [29] focused on the influence of structural parameters on PEMFC performance in horizontal fluctuation structure. The results showed that the geometric parameters near the crest of the fluctuation structure greatly influenced the performance of the flow channel, and the performance of the flow channel with the same slope was improved by 19.53%.

At the same time, the influences of the period on PEMEC performance were also found by Majasan et al. [30] in some periodic channels. Based on the electrochemical performance results, the fluid residence time was enhanced in the serpentine channel with periodic structures in the horizontal plane to show a superior electrolytic performance. Similarly, Li et al. [31] also studied the influence of horizontally periodic arrangement on the electrolytic performance of PEMEC. The results showed that a better electrolytic performance was able to be obtained by more periodic structures. But if these periodic structures were too many, the channel would be excessively elongated and the performances of PEMEC would also be reduced by consequent bubble accumulation.

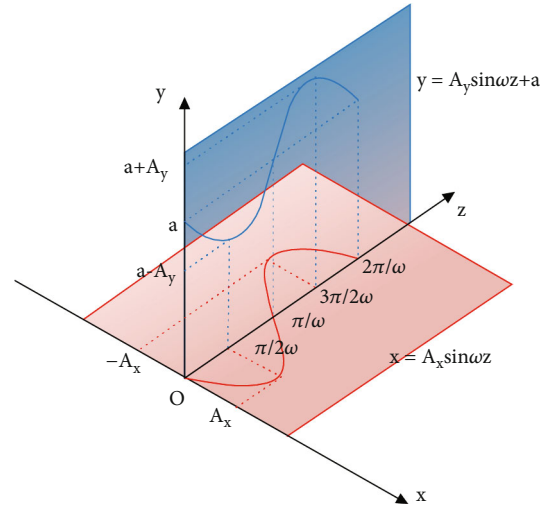


FIGURE 1: Sinusoidal functions in the horizontal and vertical planes.

Subsequently, with both the fluctuations and periodicities taken together into consideration in the horizontal flow channel, Tijani et al. [32] further found that the fluid slowed down around periodic fluctuations of the channel was more conducive to the interaction between the reactants and the MEA. The importance of the periodic fluctuation structure in the horizontal plane is also shown. At the same time, it should be pointed out that the current research on the fluctuations and periodicities in the horizontal plane is only limited to the horizontal plane, and the lack of periodic fluctuation structure in the vertical plane will also bring the insufficiencies of the research.

The researches on periodic fluctuations are mainly focused on the single horizontal [33, 34] or vertical layout [35], while the orthogonal structures in both horizontal and vertical planes at the same time are rarely studied. Therefore, a periodic fluctuation structure can be introduced into the flow channel design of PEMEC. The effect of periodic fluctuations on PEMEC performance is studied by coupling two independent sinusoidal functions on both the horizontal and vertical planes. The sinusoidal function of both planes is shown in Figure 1.

In this study, a three-dimensional and steady-state model is established by coupling the orthogonal structure with both periodic fluctuations in the horizontal and vertical planes. The PEMEC model is constructed and solved utilizing the commercial software COMSOL Multiphysics 5.6. The amplitude and angular frequency of the sinusoidal function are taken into account as geometric variables of the channel in this study. The opposite fluctuations are also considered in the horizontal plane to enhance the degree of fluctuation variation. The effects of horizontally, vertically, and orthogonally sinusoidal channel designs on the electrochemical performance and mass transfer capacity of PEMEC are studied. The four parameters containing the amplitude and angular frequency of the sinusoidal function in both the horizontal and vertical planes are derived from mathematic expressions and discussed with simulation results. Based on these parameters, 24 cases in 8 groups of experiments

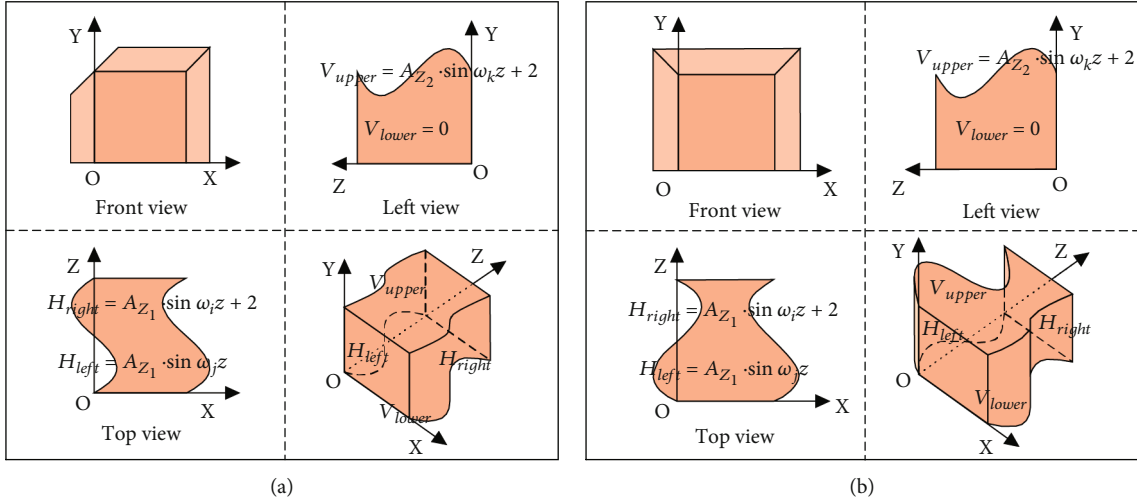


FIGURE 2: Schematic diagram of the minimum repeating unit of the flow channel in space. (a) Fluctuation with the same frequency. (b) Fluctuation with the opposite frequency.

are conducted to compare these effects in the horizontal and vertical planes, respectively. Finally, an orthogonally sinusoidal flow channel is formed by coupling the horizontally and vertically sinusoidal functions. The impact of these four parameters on all the performances of PEMEC, such as polarization curves, current density, molar fractions of hydrogen and oxygen, liquid water content, and velocity distribution, are assessed through simulations. Through the comprehensive study of spatially periodic fluctuations in this paper, a new design idea for the flow channel in PEMEC is provided to potentially help in further research.

2. Model Description

2.1. Design of Orthogonally Sinusoidal Flow Channel. As the flow channel exhibits periodic fluctuations along its length, the minimum repetitive units of the orthogonally sinusoidal flow channel are selected as the research object in Figures 2(a) and 2(b). The width direction of the flow channel is along the x -axis direction, while the height direction of the flow channel is along the y -axis one. All the repetition units will be periodically repeated along the z -axis direction from $z = 0$ to 50 mm. With the left and top views of the orthogonally sinusoidal flow channel projected to the YOZ and the XOZ planes, respectively, the curves of the walls projected can be seen as sinusoidal (S) or linear (L) curves with independent variable z . Since both the fluctuations and periodicities are governed by the crucial geometric characteristics of these walls, V_{upper} and V_{lower} are used to represent the curves of upper and lower walls in the left view, while H_{left} and H_{right} stand for the ones of left and right walls in the top view.

The flow channel design is described based on four curves. Then, the sinusoidal curve controlled by amplitude (A) and angular frequency (ω) can be expressed in a more distinguishable way as follows:

$$H_{left} = A_{z_1} \cdot \sin \omega_j z, \quad (1)$$

where A_{z_1} and ω_j are the amplitude and the angular frequency of the left wall curve function, respectively.

The height of the channel bottom is defined as zero. Limited by the width and height of the channel, the equations of the lower, upper, and right wall curve functions are as follows:

$$V_{lower} = 0, \quad (2)$$

$$V_{upper} = A_{z_2} \cdot \sin \omega_k z + 2, \quad (3)$$

$$H_{right} = A_{z_1} \cdot \sin \omega_i z + 2, \quad (4)$$

where A_{z_1} and A_{z_2} are used to represent the amplitudes of the right and upper wall curve functions, respectively. ω_i and ω_k represent the angular frequencies of the right wall and upper wall curve functions, respectively. Considering that the number of equations is too complicated to describe the characteristic curve of the minimum repetitive unit, the difference between the curve equations of the right and left walls is H , and the difference between the curve equations of the upper and lower is V , these two differences can be explained by

$$H = H_{right} - H_{left}, \quad (5)$$

$$V = V_{upper} - V_{lower}. \quad (6)$$

After substituting Eqs. (1) and (2) into Eqs. (5) and (6), Eq. (7) is received as follows:

$$H = H_{right} - H_{left} = A_{z_1} \cdot \sin \omega_i z - A_{z_1} \cdot \sin \omega_j z + 2, \quad (7)$$

$$V = V_{upper} - V_{lower} = A_{z_2} \cdot \sin \omega_k z + 2 - 0 = A_{z_2} \cdot \sin \omega_k z + 2. \quad (8)$$

Since the angular frequencies of the left and right walls curve in the horizontal plane can be the same or the opposite of each other, the same angular frequencies $\omega_i = \omega_j$ in

Figure 2(a) and the opposite ones $\omega_i = -\omega_j$ in Figure 2(b) are both shown together.

In order to explore the influence of the amplitude (A) and angular frequency (ω) on the performance of single-channel PEMEC, the channels with different geometrical parameters are divided into 8 groups and 24 cases. The characteristics of the channel are further described by some symbols. S and L are used to represent the sinusoidal and linear curves of the walls projected, respectively. In order to avoid ambiguity in the following discussion, the descriptions of the same or opposite angular frequency of the left and right wall curves are called the same or opposite frequency. Therefore, when the frequency of the left wall curve is opposite to that of the right wall curve, the left wall curve can be further named \hat{S} .

The naming rule equation for groups is as follows:

$$\text{Group[no.of group]} = \omega \text{ with different positions and sizes [no.of case]} \begin{bmatrix} V_{\text{upper}} \\ H_{\text{left}} & H_{\text{right}} \\ V_{\text{lower}} \end{bmatrix}, \quad (9)$$

where no.of group can be 1, 2, 3, 4, 5, 6, 7, or 8; no.of case can be 1, 2, 3, 4, or 5; V_{upper} can be S or L ; V_{lower} are always L ; H_{left} can be \hat{S} , S , or L ; H_{right} can be S or L ; and ω with different positions and sizes can be $2\omega_i$ or $2\omega_k$.

The amplitude and angular frequency are considered as variables to study the fluctuation and period, respectively. The grouping of the main groups in the above naming is shown in Table 1, which can be combined with Eq. (7) for a detailed explanation.

- (1) When $A_{z_1} = 0$ and $A_{z_2} = 0$, the horizontal and vertical planes are linear geometric features in Group 1
- (2) When $A_{z_1} = 0$, $A_{z_2} \neq 0$, and $\omega_k \neq 0$, the flow channels have sinusoidal geometric features in the vertical plane, while in the horizontal plane, there are still linear geometric features in Group 2
- (3) When $A_{z_1} \neq 0$, $A_{z_2} = 0$, and $\omega_i = \omega_j$, the vertical plane of the flow channels is a linear geometric feature, and the horizontal plane is sinusoidally geometric features of the left and right walls with the same frequency in Group 3
- (4) When $A_{z_1} \neq 0$, $A_{z_2} \neq 0$, and $\omega_i = \omega_j = \omega_k$, the angular frequencies of the flow channels in both vertical and horizontal planes are equal, and the left and right wall curve frequencies in the horizontal planes are the same in Group 4
- (5) When $A_{z_1} = A_{z_2} \neq 0$ and $\omega_i = \omega_j \neq \omega_k$, the amplitudes in both vertical and horizontal planes are equal, and the left and right wall curve frequencies in the horizontal plane are the same. However, the angular fre-

quency in the vertical plane is different from that in the horizontal ones in Group 5

- (6) When $A_{z_1} \neq 0$, $A_{z_2} = 0$, and $\omega_i = -\omega_j$, the vertical plane of the flow channels is a linear geometric feature, and the left and right wall curve frequencies in the horizontal plane are opposite to each other in Group 6
- (7) When $A_{z_1} \neq 0$, $A_{z_2} \neq 0$, and $\omega_i = -\omega_j = \omega_k$, the angular frequencies of the flow channels in both the vertical and horizontal planes are the same, too. However, the left and right wall curve frequencies in the horizontal plane are opposite to each other in Group 7
- (8) When $A_{z_1} = A_{z_2} \neq 0$ and $\omega_i = -\omega_j \neq \omega_k$, the amplitudes in both vertical and horizontal planes are the same, while the frequencies of the left and right wall curves are opposite in the horizontal plane. The angular frequency in the vertical plane is different from those in the horizontal ones in Group 8

Based on the groups above, the groups are further subdivided into 24 cases with amplitudes and angular frequencies in orthogonal space. The abbreviation for each case is named as follows:

$$\text{Case abbreviation} = \text{case[no.of group]} - [\text{no.of case}] \quad (10)$$

The detailed naming and geometric parameters of the single channel in each case are shown in Table 2.

2.2. Physical Model. Figure 3 shows a single channel in the PEMEC. The main structure from top to bottom includes an anode bipolar plate (ABP), anode flow channel (ACH), anode gas diffusion layer (AGDL), anode catalytic layer (ACL), proton exchange membrane (PEM), cathode catalytic layer (CCL), cathode gas diffusion layer (CGDL), cathode flow channel (CCH), and cathode bipolar plate (CBP). The geometric parameters and operating conditions of PEMEC are shown in Tables 3 and 4, respectively.

2.3. Numerical Model. Due to the complex chemical reactions and physical changes in PEMEC, the simulation study cannot be carried out individually in a short time. Therefore, with the ignoring of the nonessential factors, some assumptions of the simplified model are applied as follows [36, 41–43]:

- (1) The water in PEMEC is always the liquid state without phase transition during the reaction
- (2) All fluids in PEMEC are laminar because of the small Reynolds number
- (3) The diffusion layer, catalytic layer, and proton exchange membrane are homogeneous and isotropic mediums

TABLE 1: Symbolic description and minimum unit diagram of groups.

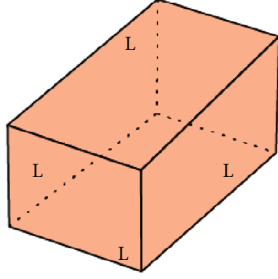
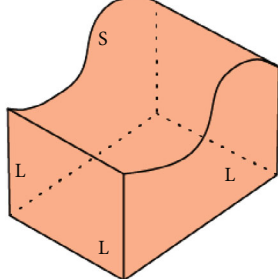
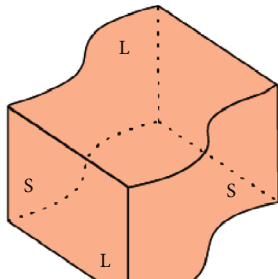
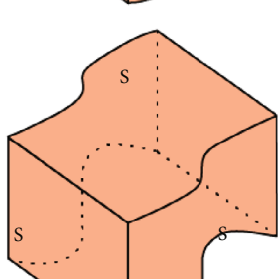
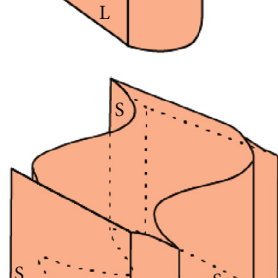
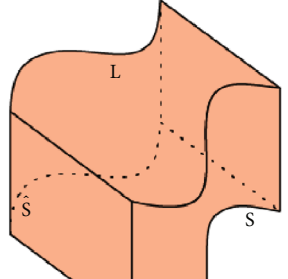
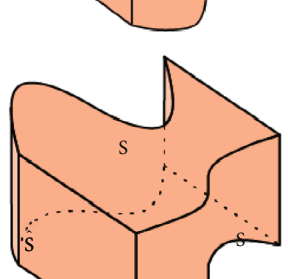
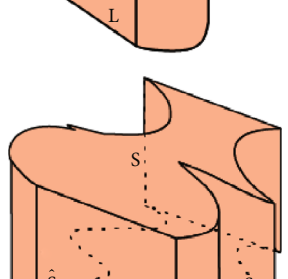
Group	Symbolic description	Minimum unit diagram
Group 1	$[\text{No.}] \begin{bmatrix} L & L \\ L & L \\ L & L \end{bmatrix}$	
Group 2	$[\text{No.}] \begin{bmatrix} S & L \\ L & L \\ L & L \end{bmatrix}$	
Group 3	$[\text{No.}] \begin{bmatrix} L & S \\ S & S \\ L & L \end{bmatrix}$	
Group 4	$[\text{No.}] \begin{bmatrix} S & S \\ S & S \\ L & L \end{bmatrix}$	
Group 5	$\omega[\text{No.}] \begin{bmatrix} S & S \\ S & S \\ L & L \end{bmatrix}$	

TABLE 1: Continued.

Group	Symbolic description	Minimum unit diagram
Group 6	$[\text{No.}] \begin{bmatrix} L & S \\ \hat{S} & S \\ L & L \end{bmatrix}$	
Group 7	$[\text{No.}] \begin{bmatrix} S & S \\ \hat{S} & S \\ L & L \end{bmatrix}$	
Group 8	$\omega[\text{No.}] \begin{bmatrix} S & S \\ \hat{S} & S \\ L & L \end{bmatrix}$	

- (4) The gaseous products obtained by the electrochemical reaction are all incompressible fluids
- (5) The cross-permeation of hydrogen and oxygen in the proton exchange membrane is ignored
- (6) The contact resistances between each part are ignored

2.3.1. *Transfer and Conservation of Electric Charges.* The Butler-Volmer equation is as follows [44]:

$$\begin{aligned}
 i_{v,a} &= a_{v,a} i_{0,a} \left(\exp \left(\frac{\alpha_a F \eta_a}{RT} \right) - \exp \left(\frac{-\alpha_c F \eta_c}{RT} \right) \right), \\
 i_{v,c} &= a_{v,c} i_{0,c} \left(\exp \left(\frac{\alpha_a F \eta_a}{RT} \right) - \exp \left(\frac{-\alpha_c F \eta_c}{RT} \right) \right),
 \end{aligned} \tag{11}$$

where $i_{v,a}$ and $i_{v,c}$ represent the local electrochemical reaction rates. $a_{v,a}$ and $a_{v,c}$ denote the electrochemically specific active surface areas. $i_{0,a}$ and $i_{0,c}$ represent the reference

TABLE 2: Dimension of a single channel in different cases.

Group	Case	Case abbreviation	A_{z_1}	A_{z_2}	ω_i	ω_k
Group 1	1 $\begin{bmatrix} L \\ L \\ L \end{bmatrix}$	1-1	0	0	0	0
	1 $\begin{bmatrix} S \\ L \\ L \end{bmatrix}$	2-1	0	0.2	$4\pi/5$	$4\pi/5$
Group 2	2 $\begin{bmatrix} S \\ L \\ L \end{bmatrix}$	2-2	0	0.5	$4\pi/5$	$4\pi/5$
	3 $\begin{bmatrix} S \\ L \\ L \end{bmatrix}$	2-3	0	0.8	$4\pi/5$	$4\pi/5$
	1 $\begin{bmatrix} L \\ S \\ L \end{bmatrix}$	3-1	0.2	0	$4\pi/5$	$4\pi/5$
Group 3	2 $\begin{bmatrix} L \\ S \\ L \end{bmatrix}$	3-2	0.5	0	$4\pi/5$	$4\pi/5$
	3 $\begin{bmatrix} L \\ S \\ L \end{bmatrix}$	3-3	0.8	0	$4\pi/5$	$4\pi/5$
	1 $\begin{bmatrix} S \\ S \\ L \end{bmatrix}$	4-1	0.2	0.5	$4\pi/5$	$4\pi/5$
Group 4	2 $\begin{bmatrix} S \\ S \\ L \end{bmatrix}$	4-2	0.8	0.5	$4\pi/5$	$4\pi/5$
	3 $\begin{bmatrix} S \\ S \\ L \end{bmatrix}$	4-3	0.5	0.2	$4\pi/5$	$4\pi/5$
	4 $\begin{bmatrix} S \\ S \\ L \end{bmatrix}$	4-4	0.5	0.8	$4\pi/5$	$4\pi/5$
	5 $\begin{bmatrix} S \\ S \\ L \end{bmatrix}$	4-5	0.5	0.5	$4\pi/5$	$4\pi/5$

TABLE 2: Continued.

Group	Case	Case abbreviation	A_{z_1}	A_{z_2}	ω_i	ω_k
Group 5	$_{2\omega_k} 5 \begin{bmatrix} S \\ S \\ L \end{bmatrix}$	5-1	0.5	0.5	$4\pi/5$	$8\pi/5$
	$_{2\omega_i} 5 \begin{bmatrix} S \\ S \\ L \end{bmatrix}$	5-2	0.5	0.5	$8\pi/5$	$4\pi/5$
Group 6	1 $\begin{bmatrix} \hat{S} \\ L \\ L \end{bmatrix}$	6-1	0.2	0	$4\pi/5$	$4\pi/5$
	2 $\begin{bmatrix} \hat{S} \\ L \\ L \end{bmatrix}$	6-2	0.5	0	$4\pi/5$	$4\pi/5$
	3 $\begin{bmatrix} \hat{S} \\ L \\ L \end{bmatrix}$	6-3	0.8	0	$4\pi/5$	$4\pi/5$
Group 7	1 $\begin{bmatrix} \hat{S} \\ L \\ S \end{bmatrix}$	7-1	0.2	0.5	$4\pi/5$	$4\pi/5$
	2 $\begin{bmatrix} \hat{S} \\ L \\ S \end{bmatrix}$	7-2	0.8	0.5	$4\pi/5$	$4\pi/5$
	3 $\begin{bmatrix} \hat{S} \\ L \\ S \end{bmatrix}$	7-3	0.5	0.2	$4\pi/5$	$4\pi/5$
	4 $\begin{bmatrix} \hat{S} \\ L \\ S \end{bmatrix}$	7-4	0.5	0.8	$4\pi/5$	$4\pi/5$
	5 $\begin{bmatrix} \hat{S} \\ L \\ S \end{bmatrix}$	7-5	0.5	0.5	$4\pi/5$	$4\pi/5$
Group 8	$_{2\omega_k} 5 \begin{bmatrix} \hat{S} \\ L \\ S \end{bmatrix}$	8-1	0.5	0.5	$4\pi/5$	$8\pi/5$
	$_{2\omega_i} 5 \begin{bmatrix} \hat{S} \\ L \\ S \end{bmatrix}$	8-2	0.5	0.5	$8\pi/5$	$4\pi/5$

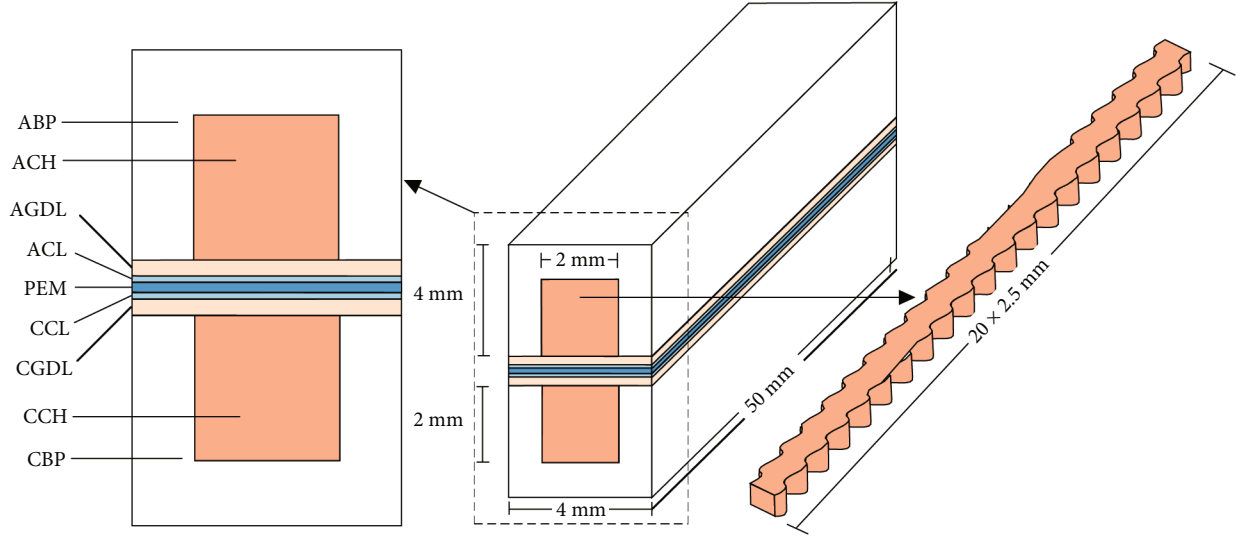


FIGURE 3: PEMEC structure diagram.

TABLE 3: Geometric parameters of PEMEC [36, 37].

Parameter	Unit	Value
Channel length	mm	50
Channel width	mm	2
Channel height	mm	2
Bipolar plate height	mm	4
Width of GDL/CL/PEM	mm	4
GDL thickness	μm	300
CL thickness	μm	20
Membrane thickness	μm	178

exchange current densities at the anode and cathode catalytic layers, respectively. α_a and α_c denote the charge transfer coefficient. η_a and η_c are the activation overpotential of the anode and cathode, respectively.

$$\begin{aligned}\eta_a &= \varphi_s - \varphi_m - E_{\text{eq}}, \\ \eta_c &= \varphi_s - \varphi_m,\end{aligned}\quad (12)$$

where φ_s is the solid overpotential, φ_m represents the electrolyte overpotential, and E_{eq} denotes the equilibrium potential.

The equilibrium potential is calculated by the Nernst equation [45] as follows:

$$E_{\text{eq}} = E_{\text{eq.ref}}(T) + \frac{RT}{nF} \ln \left(\frac{p_{\text{O}_2}^{0.5} p_{\text{H}_2}}{p_{\text{H}_2\text{O}}} \right), \quad (13)$$

where $E_{\text{eq.ref}}(T)$ can be obtained from the equation below [46].

$$E_{\text{eq.ref}}(T) = 1.229 - 0.9 \times 10^{-3}(T - 298.15), \quad (14)$$

where T represents the operating temperature of the electrolytic cell, R is the universal gas constant, F denotes the Faraday constant, and p_i (i stands for O_2 , H_2 , and H_2O) represents the respective equilibrium pressure of each substance.

2.3.2. *Proton and Electron Transport Equations.* The proton and charge transport equations are as follows [37]:

$$\begin{aligned}\nabla \cdot i_s &= \nabla \cdot (-\sigma_s \nabla \varphi_s) = S_s, \\ \nabla \cdot i_m &= \nabla \cdot (-\sigma_m \nabla \varphi_m) = S_m,\end{aligned}\quad (15)$$

where σ_s represents the electron conductivity of the solid phase electrode, σ_m is the proton conductivity of the proton exchange membrane, and S_s and S_m refer to the source terms of solid overpotential and electrolyte overpotential, respectively.

The proton conductivity of a proton exchange membrane is a function of water content and temperature [47].

$$\sigma_m = (0.0015139\lambda - 0.00326) \exp \left(1268 \left(\frac{1}{303} - \frac{1}{T} \right) \right). \quad (16)$$

2.3.3. *Conservation of Mass and Momentum.* The continuity equation is as follows [48]:

$$\nabla \cdot (\rho_l u_l) = S_l, \quad (17)$$

where ρ_l is the density of liquid water, u_l represents the velocity vector of liquid water, and S_l denotes the source term of liquid-phase mass conservation.

$$\nabla \cdot (\rho_g u_g) = S_g, \quad (18)$$

TABLE 4: Operating parameters and physical properties of PEMEC [36, 38–40].

Parameter	Value
Anode reference exchange current density, $i_{0,a}$ (A/m ²)	0.1
Cathode reference exchange current density, $i_{0,c}$ (A/m ²)	1×10^4
Anode charge transfer coefficient, α_a	0.5
Cathode charge transfer coefficient, α_c	0.5
GDL porosity, $\varepsilon^p_{\text{GDL}}$	0.5
CL porosity, $\varepsilon^p_{\text{CL}}$	0.25
GDL permeability, κ_{GDL} (m ²)	1×10^{-12}
CL permeability, κ_{CL} (m ²)	1×10^{-13}
Liquid water density, ρ_l (kg/m ³)	998
Liquid water dynamic viscosity, μ_l (Pa·s)	3.55×10^{-4}
Oxygen dynamic viscosity, μ_{O_2} (Pa·s)	2.34×10^{-5}
Hydrogen dynamic viscosity, μ_{H_2} (Pa·s)	8.915×10^{-6}
Inlet temperature, T (K)	353.15
Inlet flow rate, u (m/s)	0.125
Outlet pressure, P (atm)	1
Anode reference specific surface area, $a_{v,a}$ (1/m)	1×10^6
Cathode reference specific surface area, $a_{v,c}$ (1/m)	1×10^6
Thermal conductivity of the membrane, k_m (W·m ⁻¹ ·K ⁻¹)	0.21
Heat capacity of the membrane, $C_{p,m}$ (J·kg ⁻¹ ·K ⁻¹)	1090

where ρ_g is the density of the gas, u_g represents the velocity vector of the gas, and S_g denotes the mass source term of a gas produced by a chemical reaction.

The momentum conservation equation is as follows [49]:

$$\begin{aligned} \frac{\rho_l}{\varepsilon^p} (u_l \cdot \nabla) \frac{u_l}{\varepsilon^p} &= \nabla \cdot [-p_l I + K] - \left(\frac{\mu_l}{\kappa} + \beta \rho |u_l| + \frac{S_m}{(\varepsilon^p)^2} \right) u_l, \\ K &= \frac{\mu_l}{\varepsilon^p} (\nabla u_l + (\nabla u_l)^T) - \frac{2}{3} \frac{\mu_l}{\varepsilon^p} (\nabla \cdot u_l) I, \\ \rho_l \nabla \cdot u_l &= S_m, \end{aligned} \quad (19)$$

where κ is the permeability of porous media, ε^p denotes the porosity of porous media, I denotes the transposition symbol, p_l is the liquid water pressure, and μ_l represents the dynamic viscosity of liquid water.

$$\begin{aligned} \frac{\rho_g}{\varepsilon^p} (u_g \cdot \nabla) \frac{u_g}{\varepsilon^p} &= \nabla \cdot [-p_g I + K] - \left(\frac{\mu_g}{\kappa} + \beta \rho |u_g| + \frac{S_m}{(\varepsilon^p)^2} \right) u_g, \\ K &= \frac{\mu_g}{\varepsilon^p} (\nabla u_g + (\nabla u_g)^T) - \frac{2}{3} \frac{\mu_g}{\varepsilon^p} (\nabla \cdot u_g) I, \\ \rho_g \nabla \cdot u_g &= S_m, \end{aligned} \quad (20)$$

where κ is the permeability of porous media, ε^p denotes the porosity of porous media, I denotes the transposition sym-

bol, p_g is the gas pressure, and μ_g represents the dynamic viscosity of the gas.

2.3.4. Transport of Energy. The energy equation in all computational domains is defined as follows [50]:

$$\nabla \cdot (\rho_{\text{eff}} C_{p,\text{eff}} u T) = \nabla \cdot (k_{\text{eff}} \nabla T) + S_T, \quad (21)$$

where ρ_{eff} , $C_{p,\text{eff}}$, and k_{eff} stand for the effective density, the effective heat capacity, and the effective thermal conductivity, respectively, which can be calculated as follows [51]:

$$\begin{aligned} \rho_{\text{eff}} &= (1 - \varepsilon^p) \rho_s + \varepsilon^p \rho_f, \\ C_{p,\text{eff}} &= (1 - \varepsilon^p) C_{p,s} + \varepsilon^p C_{p,f}, \\ k_{\text{eff}} &= (1 - \varepsilon^p) k_s + \varepsilon^p k_f, \end{aligned} \quad (22)$$

where ρ_s , $C_{p,s}$, and k_s are the density, heat capacity, and thermal conductivity of the solid matrix, respectively. ρ_f , $C_{p,f}$, and k_f are the density, heat capacity, and thermal conductivity of the fluid, respectively. S_T denotes the source term of the energy equation, which includes the irreversible reaction heat and entropic heat generated during the electrolytic reaction, as well as ohmic heat generated in the electrode and membrane. Table 5 shows the source terms in the governing equation.

2.4. Boundary Conditions. In this study, the PEMEC channel is operated at a temperature of 353.15 K, and the working pressure of the outlet is set to 1 atm. Only liquid water is introduced into the inlets of both the anode and cathode channels,

TABLE 5: Source terms in the governing equations.

Descriptions of the source term	Source term
Source term of solid overpotential	$S_s = \begin{cases} i_v, \text{ACL} \\ -i_v, \text{CCL} \end{cases}$
Source term of electrolyte overpotential	$S_m = \begin{cases} -i_v, \text{ACL} \\ i_v, \text{CCL} \end{cases}$
Source term of liquid-phase mass conservation	$S_l = - i_v M_{\text{H}_2\text{O}}/2F, \text{ACL}$
Source term of gas-phase mass conservation	$S_g = \begin{cases} S_{\text{O}_2} = i_v M_{\text{O}_2}/4F, \text{ACL} \\ S_{\text{H}_2} = i_v M_{\text{H}_2}/2F, \text{CCL} \end{cases}$
Source term of energy equation	$S_T = \begin{cases} \sigma_s(\nabla\varphi_s)^2, \text{BP} \\ \sigma_s(\nabla\varphi_s)^2, \text{GDLs} \\ \sigma_m(\nabla\varphi_m)^2, \text{PEM} \\ i_v\eta_c + \sigma_s(\nabla\varphi_s)^2 + \sigma_m(\nabla\varphi_m)^2, \text{CCL} \\ i_v\eta_a + \sigma_s(\nabla\varphi_s)^2 + \sigma_m(\nabla\varphi_m)^2 - T(dE_{\text{eq,ref}}/dT), \text{ACL} \end{cases}$

which are located on the same side with an inlet velocity of 0.125 m/s. The liquid water in the anode channel serves as the reactant and is used to promote the removal of oxygen generated, while the liquid water in the cathode channel is only used to remove hydrogen. The bipolar plate of the anode side is set to 2.2 V, and that of the cathode side is set to 0 V.

2.5. Numerical Computation Procedure. In this study, the numerical model is built in COMSOL Multiphysics 5.6 with free and porous medium flow modules and electrolyzer modules to solve the problems of charge transfer and material transfer. The iterative process is completed when the residuals of free and porous media flow modules are less than 10^{-3} , and those of the electrolyzer coupling with multi-physical fields are all less than 10^{-4} .

2.6. Model Verification. In order to verify the accuracy of the numerical model, the polarization curve obtained by numerical simulation is compared with the experimental results received by Majasan et al. [30] in Figure 4. The maximum error between the experimental results and the simulated ones is 3.1%, which proves that the numerical model established is accurate and reliable. Due to the application of the finite element method, the quality and number of grids become necessary factors affecting calculation time and accuracy [52].

When the voltage is 1.8 V, different grid numbers are selected for the simulation study, and the curves obtained are shown in Figure 5. When the number of grids is lower, the current density decreases from 446.8 mA/cm² to 446.67 mA/cm² with the grids increasing from 48500 to 106700. Unlike the lower number of grids, the current density will remain almost constant when the number is increased from 155200 to 242500. So the number of grids is selected as 155200.

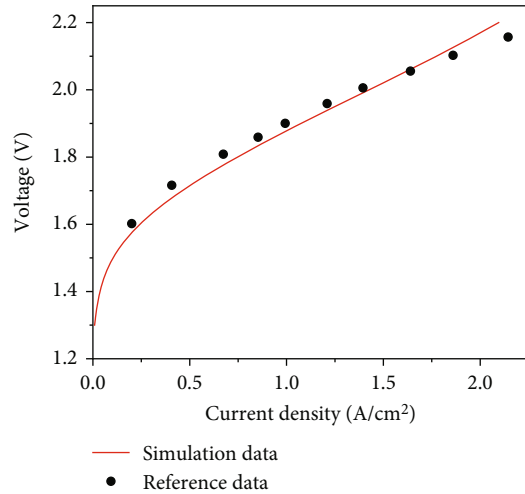


FIGURE 4: Comparisons of the polarization curve obtained from the present study and reference data.

3. Results and Discussions

3.1. Effect of Sinusoidal Curve in Vertical Plane on PEMEC Performance. The polarization curves and oxygen content curves of different Groups 1 and 2 are shown in Figures 6(a) and 6(b). When 2.0 V is selected as the standard for comparison, the polarization curves of Group 2 are better compared to Group 1 with the maximum 5.1% increment. Also, from Case 2-1, Case 2-2, and Case 2-3, the polarization performances are increased with the increasing amplitude in the vertical plane. Also, since the amplitude is too small in Case 2-1, the polarization performance of Case 2-1 in Group 2 is a little improved compared with Case 1-1. The oxygen content of Case 2-3 with the highest amplitude is reduced by about 22.3% at 40 mm away from the inlet compared with Case 1-1. Furthermore, oxygen in the diffusion layer

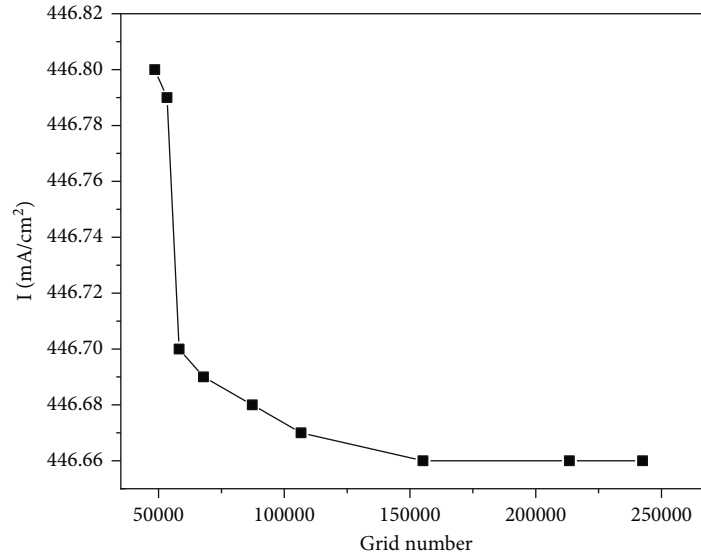


FIGURE 5: Grid independence verification.

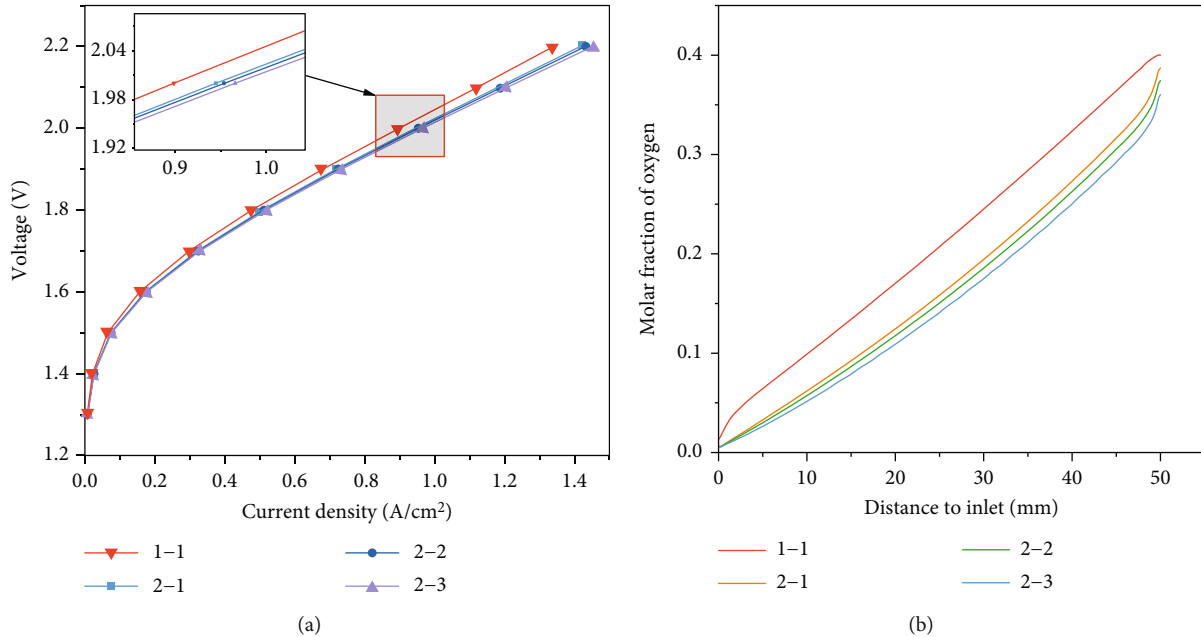


FIGURE 6: PEMEC simulation results with sinusoidal curves in the vertical plane. (a) Polarization curves of Groups 1 and 2. (b) Oxygen content at the center of AGDL along the length.

decreases with the increasing amplitude in Figure 6(b). It shows that the vertically sinusoidal structure can promote oxygen removal and change the mass transfer in the flow channel.

Figure 7(a) shows the flow channel cross-sections of Groups 1 and 2 in the YOZ plane. The overall effect of the local current density distribution in Figure 7(b) is the same as that of the polarization curve. Interestingly, it can be seen from Figure 7(b) that the current density of Group 2 is significantly higher than that of Group 1 near the inlet. The increase of outlet current density is not apparent, which can be attributed to the fact that the design of the vertically

sinusoidal curve improves the efficiency at the initial stage of the electrochemical reaction. However, due to the continuous consumption of liquid water in the process of passing through the flow channel, the effect of amplitude on improving current density at the outlet is weakened. In the vertical plane, appropriately increasing the amplitude of the sinusoidal curve is conducive to enhancing the polarization performance of PEMEC.

In order to explore the effect of the vertically sinusoidal curve on PEMEC’s mass transfer capacity, Figures 7(c) and 7(d) are selected to measure the material transport in PEMEC’s hydrogen production process. In Group 2, the

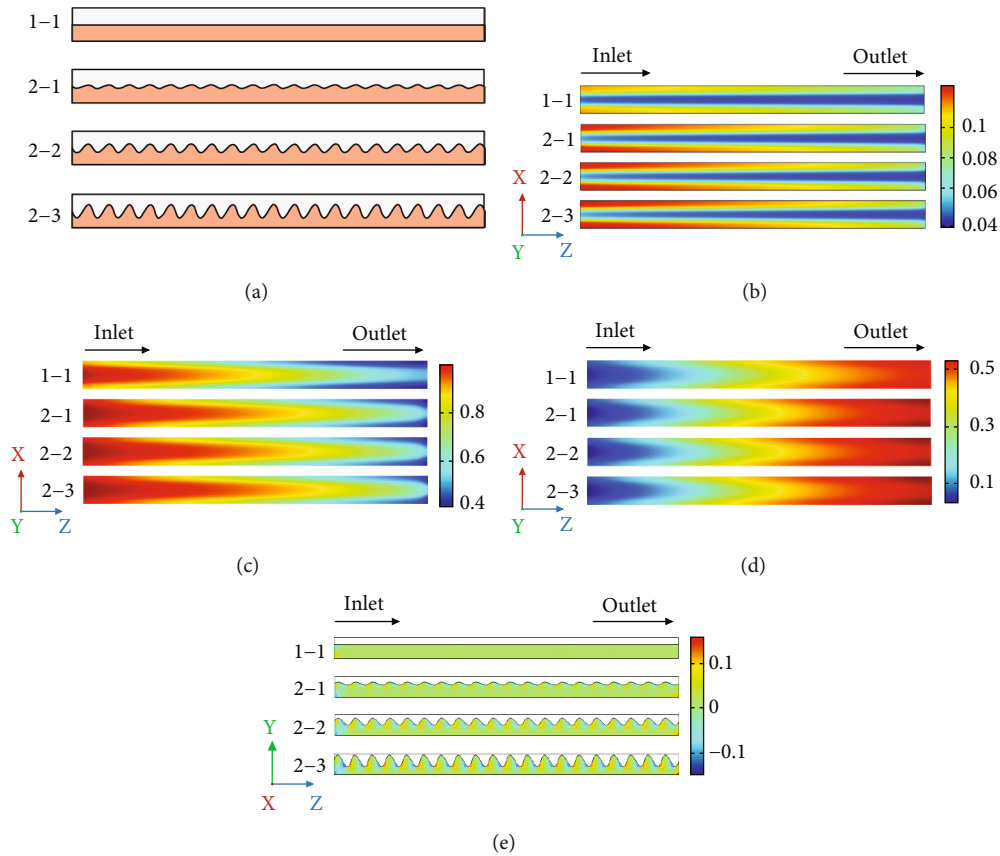


FIGURE 7: (a) Cross-section of the flow channel in the YOZ plane. (b) Contour of local current density distribution at the ACL-PEM interface (A/cm^2). (c) Contour of H_2O molar fraction at the AGDL-ACL interface. (d) Contour of H_2 molar fraction at the CCL-PEM interface. (e) Contour of vertical velocity in the middle cross-section vertical to the XOZ plane along the channel (m/s).

liquid water content at the AGDL-ACL interface and the hydrogen content at the CCL-PEM interface are both increased, and the hydrogen content of the vertically sinusoidal flow channel is increased by 8.3%, which is consistent with the change law of the polarization performance.

Figure 7(e) shows the influence of amplitude in the vertical plane on the vertical velocity. In Group 1, after the vertical velocity with 0.04 m/s is distributed at a small distance from the inlet, the vertical velocity with 0 m/s will be almost uniformly distributed along the rest of the channel. It can be proved that the flow in the noninlet region of the straight channel is parallel flow. High-speed regions positively correlated with amplitudes will appear near the trough of the vertical sinusoid in Group 2. The same finding can be obtained in the research proposed by Yan et al. [53]. In Group 2, by increasing these vertical velocities up to 0.079 m/s towards GDL at most, the mass transfer process of liquid water involved in the electrochemical reaction is accelerated to produce more oxygen and hydrogen. Therefore, it is proved that the electrolytic result can be changed by changing the sinusoidal function parameters of the periodic fluctuation structure in the vertical plane.

3.2. Effect of Sinusoidal Curve in Horizontal Plane on PEMEC Performance. To investigate the effect of the horizontally sinusoidal amplitude on the performance of

PEMEC, the polarization curves of horizontally sinusoidal channels with the same and opposite frequencies are compared in Figure 8(a). Overall, the polarization performances of Groups 3 and 6 are better than those of Group 1 because of the horizontally sinusoidal curve. At 2.0 V, the polarization performance of Case 6-3 is the best in Group 3 and Group 6, which is improved by 14.1% compared with Case 1-1. Interestingly, the polarization curve of PEMEC in horizontally sinusoidal channels is also positively correlated to amplitude. Though the frequencies of Groups 3 and 6 are different, the polarization performances with the same amplitude are almost the same.

It can be seen from Figure 8(b) that the oxygen content in the AGDL is related to the structure of the horizontally sinusoidal curve. With increasing amplitude, the oxygen content in the horizontal structure with opposite frequency decreases more significantly than that with the same frequency. Among all of the cases with opposite frequency, Case 6-3 has the lowest oxygen content. This phenomenon may be due to the varying width of the flow channel. This channel facilitates the transformation of large bubbles into smaller ones to some extent, and the oxygen can be removed more efficiently to reduce its content.

Figures 9(a) and 9(b) are schematic diagrams of horizontally sinusoidal flow channels in the XOZ plane. Figures 9(c) and 9(d) show the local current density of PEMEC with the

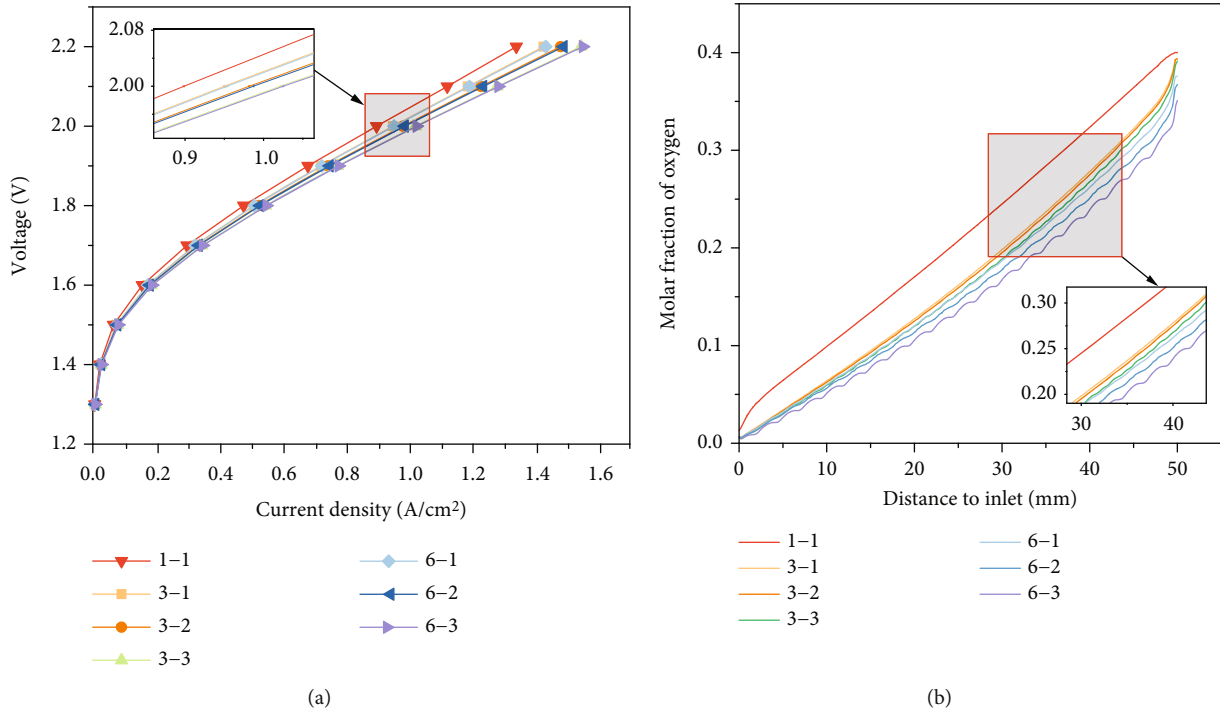


FIGURE 8: PEMEC simulation results with sinusoidal curves in the horizontal plane. (a) Polarization curve of horizontally sinusoidal curve flow channel. (b) Curve of oxygen content at the center of GDL along the length.

same and opposite frequencies at the ACL-PEM interface, respectively. In all the cases, with the increasing amplitude, the local current density at the inlet is increased to enhance the distributed area of high current density across the interface. It should be pointed out that the degree of changes caused by the horizontally sinusoidal curve is much higher than that caused by the vertically sinusoidal one. When the amplitude of the sinusoidal channel with the same frequency is 0.8 mm, the maximum local current density occurs at 0.1183 A/cm². The amplitude changes the inlet local current density of the same frequency sinusoidal curve more significantly than that of the opposite frequency one. In general, Case 6-3 shows the best polarization performance among the horizontally sinusoidal PEMEC structures. Moreover, Case 3-3 exhibits higher local current density at the inlet.

Figures 10(a)–10(d) show the influence of the horizontally sinusoidal amplitude on the internal mass transfer of PEMEC. Since the transportation laws of both oxygen and water are similar, flow channels with opposite frequencies also have a stronger ability to supply water in Figures 10(a) and 10(b). In Figures 10(c) and 10(d), the variation of hydrogen content is closely related to the variation of polarization performance. No matter whether the frequencies of horizontally sinusoidal curves are the same or opposite, the hydrogen production capacities are improved at the same level. Among them, the hydrogen content of Case 6-3 is increased by 16.13% compared with Case 1-1. In general, compared with Case 1-1, the horizontally sinusoidal curve has a great influence on the mass transfer performance of PEMEC.

The horizontal velocity distribution employed by Amit et al. [54] is used to investigate the states of fluid flow. Since

the structure is designed on the horizontal plane, the effect of the horizontally sinusoidal amplitude on the performance of PEMEC can also be studied by the horizontal velocity at the ACH-AGDL interface, as shown in Figures 11(a) and 11(b). Comparing the distribution of horizontal velocities in Group 3 and Group 6, the high-speed regions positively correlated to amplitude will be formed near both the trough of the horizontal sinusoid. This conclusion is the same as that obtained by Zhou et al. [35]. However, this region is more prominent in the same frequency channel than the opposite one. Among Group 3 with the same frequency, Case 3-3 has the largest amplitude and high-speed region, with a maximum velocity of 0.0368 m/s, which enhances the horizontal mass transfer capacity to accelerate reactant supply and product gas removal.

3.3. Effect of Orthogonally Sinusoidal Curve in Space on PEMEC Performance. The polarization curves of orthogonally sinusoidal channels with the same and opposite frequencies are shown in Figures 12(a) and 12(b), respectively. In Figure 12(a), the larger amplitude is positively related to the polarization performance of PEMEC in both horizontal and vertical planes. Different from the amplitude, the influence of angular frequencies on the polarization performance is not specific. This conclusion can be drawn from the same polarization performances in Case 5-1 and Case 4-5. In addition, by comparing both Figures 12(a) and 12(b), it can be seen that similar laws of the impact of the amplitude and angular frequency on the polarization performance of PEMEC can be obtained in orthogonally sinusoidal channels with the same frequency or opposite frequency. Overall, Case 4-2 and Case 7-2 have

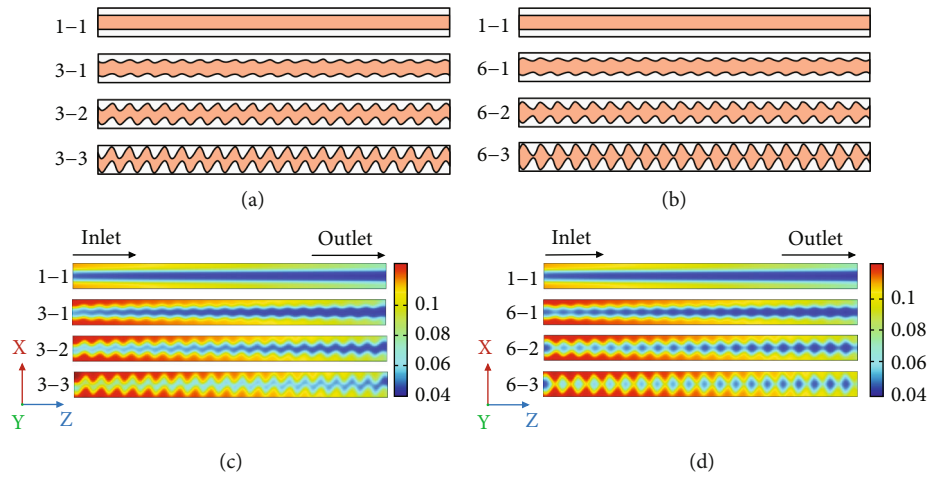


FIGURE 9: (a) Cross-section of flow channel with the same frequency in the YOZ plane. (b) Cross-section of flow channel with opposite frequency in the YOZ plane. (c) Contour of local current density distribution contour at the ACL-PEM interface for Group 3 (A/cm^2). (d) Contour of local current density distribution at the ACL-PEM interface for Group 6 (A/cm^2).

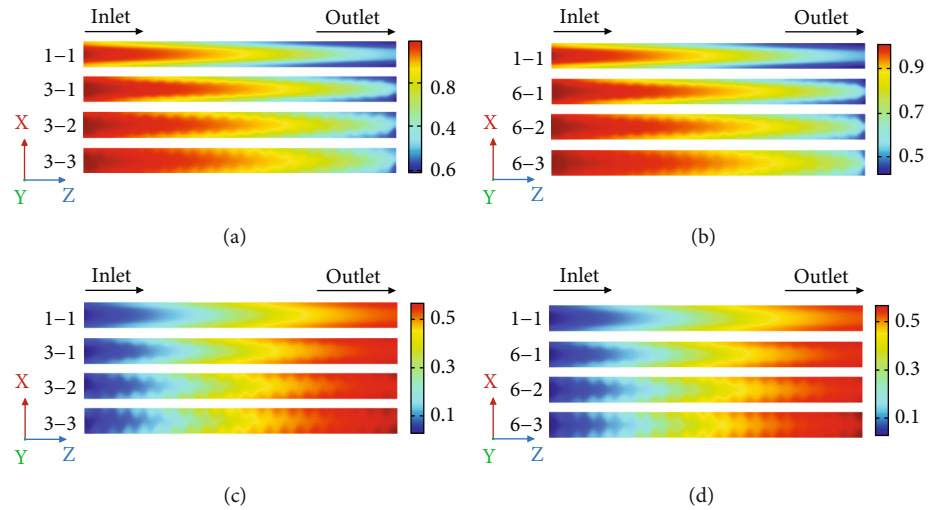


FIGURE 10: (a) Contour of H_2O molar fraction at the AGDL-ACL interface for Group 3. (b) Contour of H_2O molar fraction at the AGDL-ACL interface for Group 6. (c) Contour of H_2 molar fraction at the CCL-PEM interface for Group 3. (d) Contour of H_2 molar fraction at the CCL-PEM interface for Group 6.

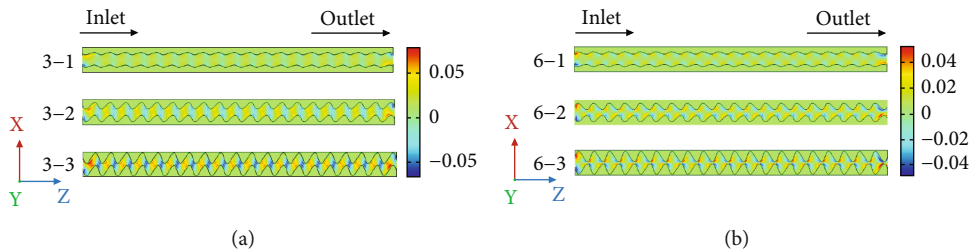


FIGURE 11: (a) Contour of horizontal velocity distribution in the XOZ plane below the flow channel for Group 3 (m/s). (b) Contour of horizontal velocity distribution in the XOZ plane below the flow channel for Group 6 (m/s).

the best polarization performance in Figures 12(a) and 12(b), respectively. Based on the 12.5% improvement in the polarization performance of Case 1-1 at 2.0 V compared with that obtained by Zhang and Xing [37], the polarization

performances of Case 4-2 and Case 7-2 are further improved by 15.66% and 16.39%, respectively. This result may be explained by the largest spatial amplitudes in these two groups. Although both Case 4-4 and Case 7-4 also exhibit

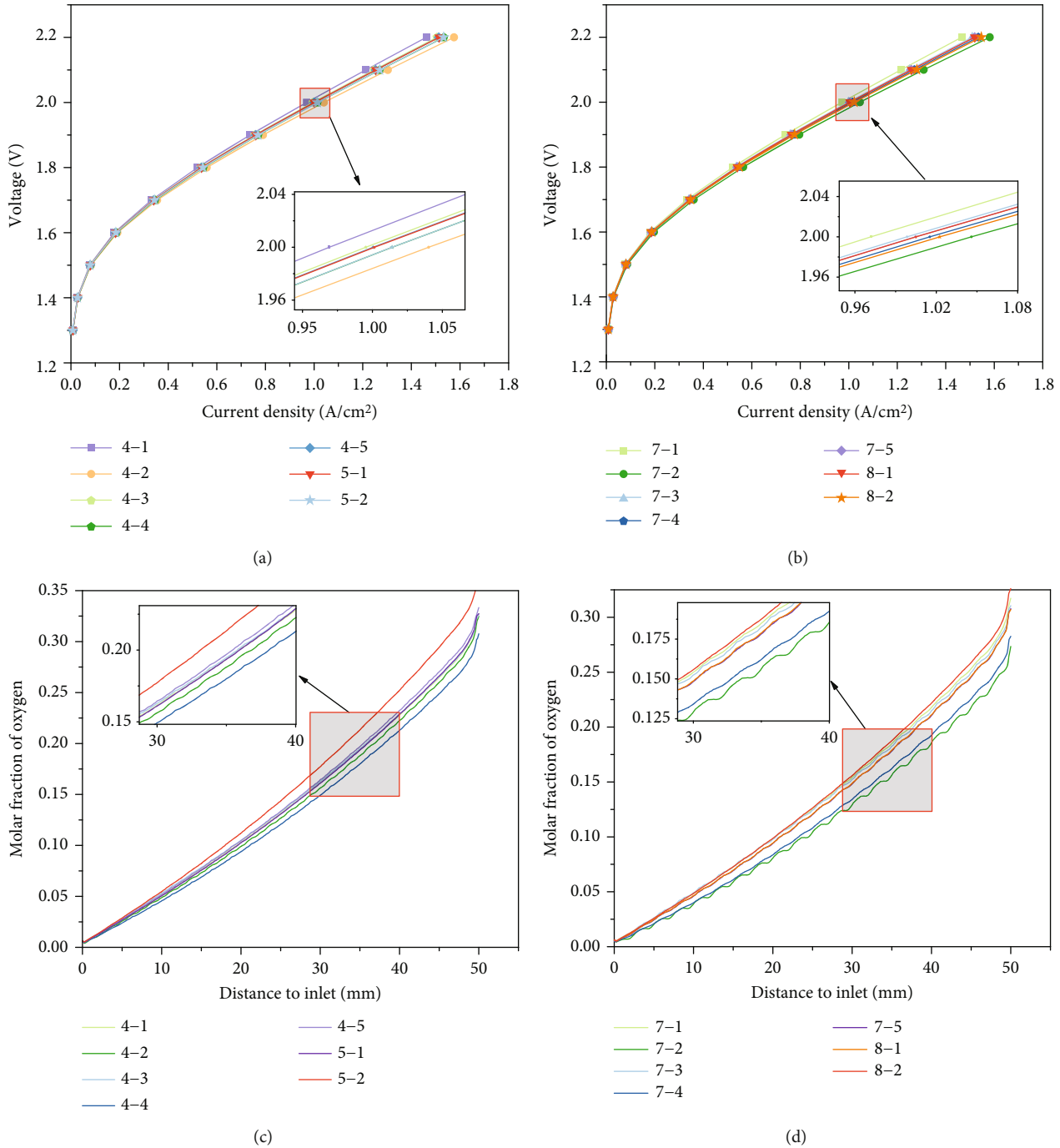


FIGURE 12: Simulation results of PEMEC with orthogonally sinusoidal structures of the same and opposite frequency. (a) Polarization curve of orthogonally sinusoidal structures with the same frequency. (b) Polarization curve of orthogonally sinusoidal structures with the opposite frequency. (c) Oxygen content curve of orthogonally sinusoidal structures with the same frequency at the center of AGDL along the length. (d) Oxygen content curve of orthogonally sinusoidal structures with the opposite frequency at the center of AGDL along the length.

the largest spatial amplitudes, the performances are lower compared to Case 4-2 and Case 7-2 due to the relatively weaker promotion from vertical plane amplitudes.

As one of the products, the oxygen content distribution will affect the mass transfer capacity of PEMEC. Figures 12(c) and 12(d) show the oxygen content curve of orthogonally sinusoidal structures with the same and opposite frequency at the center of GDL along the length, respec-

tively. The laws that the oxygen content distributions in Group 4 and Group 7 are more deeply affected by the vertical amplitudes than the horizontal ones with the same frequency, while the horizontal ones with the opposite frequency seem more significant to the oxygen content distribution obtained. Since there are the largest vertical and horizontal amplitudes in Case 4-4 with the same frequency and Case 7-2 with the opposite frequency, respectively, the

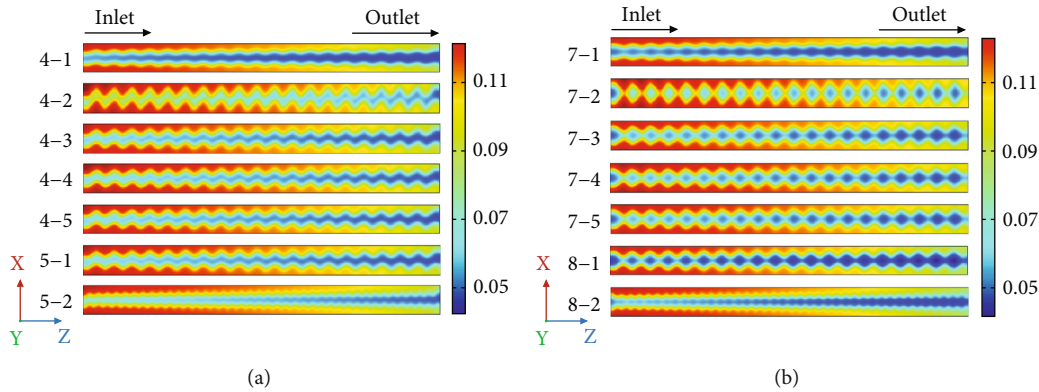


FIGURE 13: (a) Local current density distribution contour of orthogonally sinusoidal structures with the same frequency at the ACL-PEM interface (A/cm^2). (b) Local current density distribution contour of orthogonally sinusoidal structures with the opposite frequency at the ACL-PEM interface (A/cm^2).

lowest oxygen content will be shown in both cases. At a distance of 40 mm from the inlet, the oxygen content of Case 4-4 and Case 7-2 decreases by 33.87% and 42.63%, respectively, compared with Case 1-1. Besides the amplitudes, whether the same or the opposite frequency, the angular frequencies in the horizontal plane are much more critical to the oxygen content than those in the vertical one. This conclusion can be revealed by Case 4-5, Group 5, Case 7-5, and Group 8.

In order to further investigate the effects of amplitude and angular frequency on local current density in PEMEC with orthogonally sinusoidal channels, both Figures 13(a) and 13(b) are shown. In Group 4 and Group 7, similar with the polarization performance, since the local current density at the inlet of the flow channel is positively correlated with the amplitude, Case 4-2 and Case 7-2 with the largest amplitudes in the horizontal plane have the best uniform distribution of the global current density. Secondly, the effects of horizontal and vertical angular frequencies in Group 5 and Group 8 are also not specific. Compared with Case 4-5 and Case 7-5, although the angular frequencies in the vertical plane of Case 5-1 and Case 8-1 are both increased, the local current density at the inlet will be decreased. On the contrary, due to the increase of the angular frequency in the horizontal plane, the local current density at the inlet of Case 5-2 is greatly improved, while there is almost no change in Case 8-2.

Similar to the variation of oxygen content, the distribution of liquid water is also shown in Figures 14(a) and 14(b). Whether the frequencies are the same or opposite, the optimal distributions of liquid water content in horizontal planes will occur in the cases with the largest amplitudes, such as Case 4-2, Case 4-4, Case 7-2, and Case 7-4. The liquid water content of Case 7-2 surpasses that of the other three channels. Since the spatial amplitudes are the largest, the volumes of the channel are also the biggest. Then, both the transportation of the liquid water to GDL and the dispersion of the oxygen bubbles are enhanced.

The mole fraction distribution of hydrogen at the CCL-PEM interface is shown in Figures 14(c) and 14(d). From these figures, the amplitudes and angular frequencies in both horizontal and vertical planes are positively related to the

mole fraction of hydrogen. In general, there will be a higher hydrogen content in the orthogonally sinusoidal structure with the same frequency and opposite frequency. Compared with Case 1-1, the hydrogen contents of Case 4-2 and Case 7-2 are increased by 10.94% and 8.76%, respectively. In an orthogonally sinusoidal flow channel with the same frequency, the hydrogen content of Case 5-2 with high horizontal angular frequency is increased by 11.07%. The results show that the horizontal angular frequency greatly influences the hydrogen content in the same frequency orthogonally sinusoidal flow channel.

The vertical velocity in the middle cross-section vertical to the XOZ plane along the channel is illustrated in Figures 15(a) and 15(b) with contours. Firstly, the area of the high-speed region at the trough also increases with the increase of the amplitude in both horizontal and vertical planes. Because of the forced convection, the highest vertical velocities in these high-speed regions are 0.18 m/s and 0.2 m/s in Case 4-4 with the same frequency and in Case 7-4 with the opposite frequency, respectively. Secondly, with the increase of angular frequency in the vertical plane, the stronger periodicity in the flow channel makes the distributions of velocity in these high-speed regions more uniform, such as Case 5-1 and Case 8-1. However, the change of the angular frequency in the horizontal plane is not able to significantly improve the area and value of the high-speed region.

The horizontal velocity at the ACH-AGDL interface is illustrated in Figures 15(c) and 15(d) with contours. Similar to vertical velocity, the high-speed region area of the horizontal velocity also varies with the amplitude. Moreover, the maximum area of the high-speed region appears in Case 4-2 and Case 7-2, but the difference is that the area of the horizontal high-speed region with the same frequency is large enough to influence the adjacent high-speed regions [55]. With the adjacent high-speed regions overlaid with each other, the horizontal transmission of materials is extremely strengthened. The maximum horizontal velocity can be almost 0.0767 m/s in Case 4-2. In Case 5-2, more high-speed regions will be shown in the whole region, and the maximum value of 0.09 m/s will be also found near the inlet. It is shown that the horizontal angular frequency

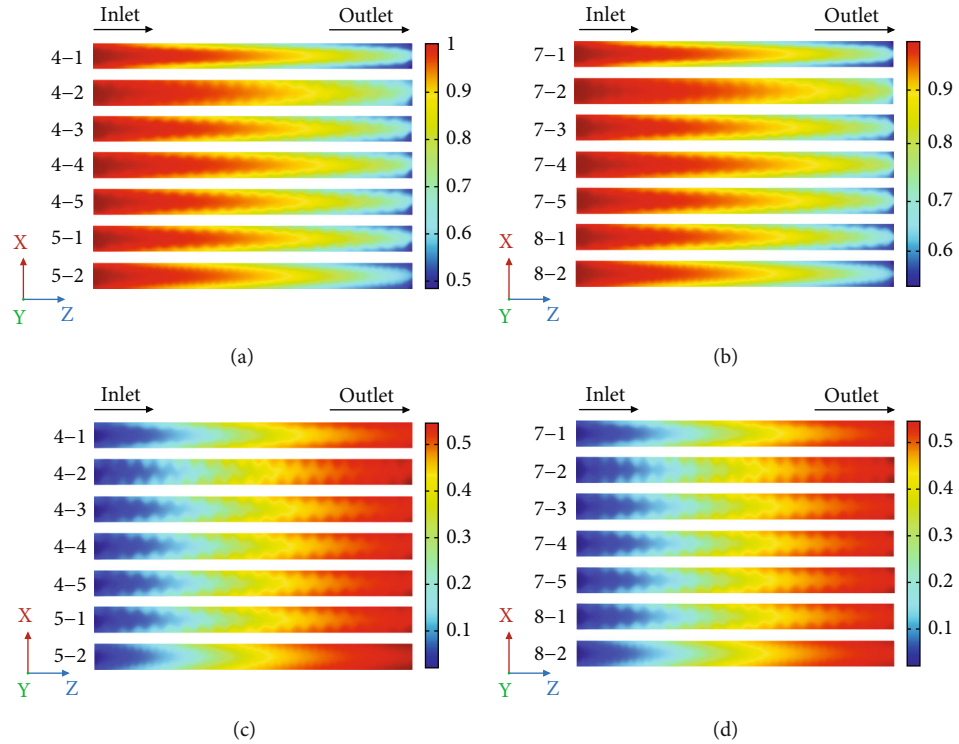


FIGURE 14: (a) H_2O molar fraction contour of orthogonally sinusoidal structures with the same frequency at the AGDL-ACL interface. (b) H_2O molar fraction contour of orthogonally sinusoidal structures with the opposite frequency at the AGDL-ACL interface. (c) H_2 molar fraction contour of orthogonally sinusoidal structures with the same frequency at the CCL-PEM interface. (d) H_2 molar fraction contour of orthogonally sinusoidal structures with the opposite frequency at the CCL-PEM interface.

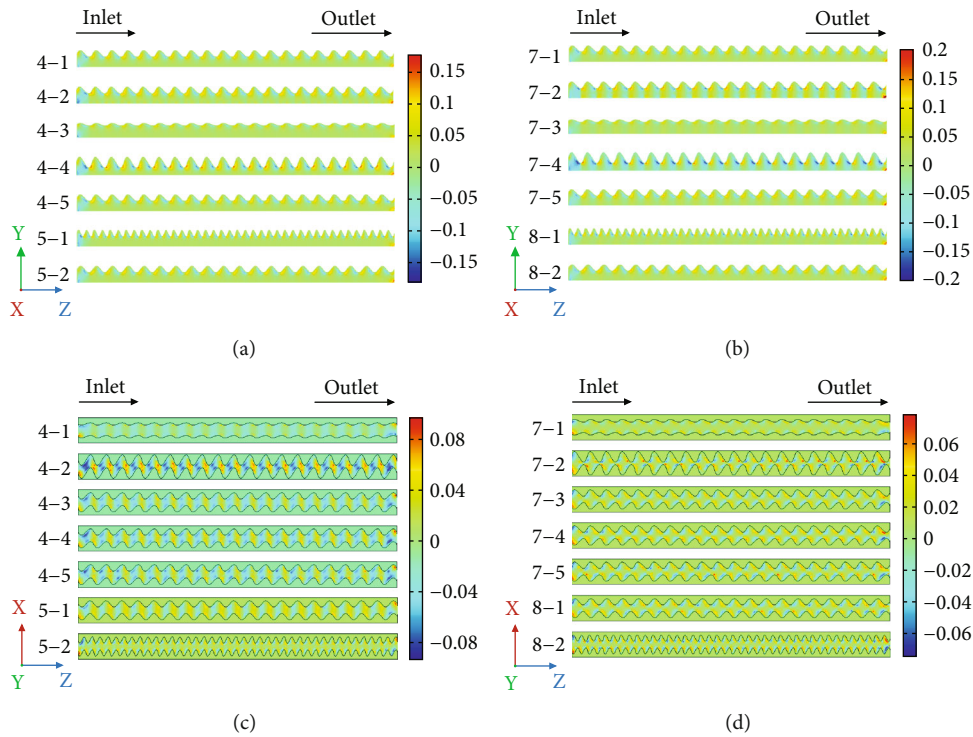


FIGURE 15: (a) Contour of vertical velocity in the middle cross-section vertical to the XOZ plane along the channel with the same frequency (m/s). (b) Contour of vertical velocity in the middle cross-section vertical to the XOZ plane along the channel with the opposite frequency (m/s). (c) Contour of horizontal velocity distribution at the ACH-AGDL interface with the same frequency (m/s). (d) Contour of horizontal velocity distribution at the ACH-AGDL interface with the opposite frequency (m/s).

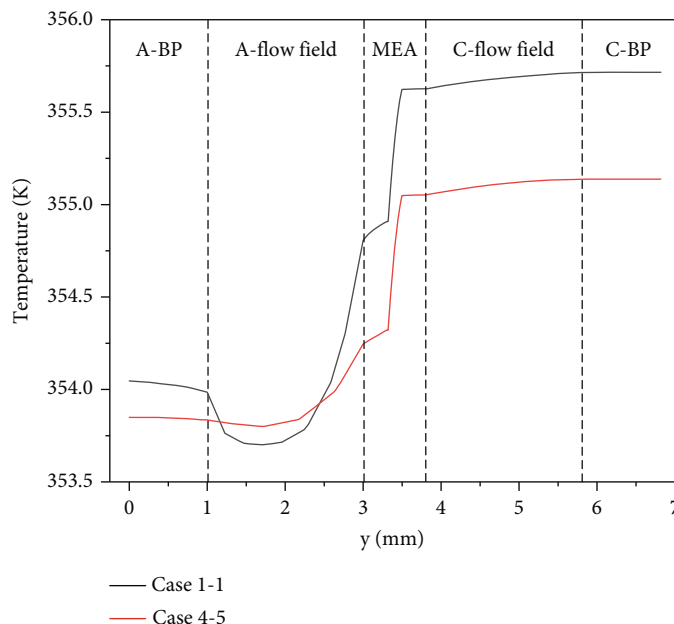


FIGURE 16: Temperature distribution curves of Case 4-5 and Case 1-1 in the y -axis direction of the PEMEC.

impacts the horizontal mass transfer of PEMEC with the same frequency. On the contrary, the vertical angular frequency only affects the number of high-speed regions but does not obtain the maximum horizontal velocity.

The lifetime and performance of the proton exchange membrane are greatly affected by the internal heat transfer performance of PEMEC. Therefore, in order to study the accuracy of heat transfer performance, the temperature distribution curves of the single channel and orthogonally sinusoidal channel along the y -axis direction of the PEMEC are shown in Figure 16. In Case 1-1, the temperature of the anode side flow field drops to a minimum of 353.70 K due to the rapid flow rate of the fluid center. The MEA is the main region of the electrolysis process, where the temperature reaches the highest value, 355.62 K. Although water is supplied to the cathode for cooling, the temperature on the cathode side is still higher than that on the anode side. The temperature distribution law of this model is the same as that obtained by Zhou et al. [48]. In addition, the overall temperature is lower than the maximum working temperature of PEMEC [56]. The results indicate that the internal heat transfer process of the model is accurate.

Case 4-5 is selected to study the influence of the orthogonally sinusoidal structure flow field on the internal heat transfer process of a single channel. Compared with Case 1-1, the maximum temperature at the MEA decreases by 0.57 K. The average temperature recorded at ACL is 0.08 K lower than the highest average temperature reported by Wang et al. [36]. The minimum temperature of the anode side is almost the same as in Case 1-1. Besides, the introduction of the orthogonally sinusoidal structure on the cathode side significantly decreases the temperature of the cathode side flow field. In analysis of both mass and heat transfer, the orthogonally sinusoidal structure enhances fluid velocity to promote material transport and heat transfer. Sui et al. also found and proved these conclusions [57]. Since some

other practical engineering problems can be solved in this novel orthogonally sinusoidal structure by effective heat dissipation performance [58, 59], the structure can be also regarded as an advantage in PEMEC.

4. Conclusions

In this study, a three-dimensional orthogonally sinusoidal flow channel model with periodicity and fluctuation is proposed. The different amplitudes and angular frequencies affect the electrochemical and mass transfer performance of PEMEC with vertically, horizontally, and orthogonally sinusoidal flow channels. The main conclusions are as follows:

- (1) The amplitude has a positive effect on the performance of the vertically sinusoidal flow channel PEMEC. Case 2-3 with the largest amplitude improves the polarization performance by 5.1% at 2.0 V, reduces the oxygen content by 22.3% at 40 mm away from the inlet, increases the maximum hydrogen content by 8.3%, and reaches the maximum vertical velocity of 0.079 m/s. The vertically sinusoidal flow channel accelerates the material transport process to supply the reactant and remove the products
- (2) The amplitude greatly influences the hydrogen production performance of the horizontally sinusoidal flow channel. Compared with the same frequency structure, the hydrogen content of Case 6-3 is higher than that of Case 3-3 by 16.13% due to the change in the width of the fluid flow direction
- (3) Both spatial amplitude and angular frequency affect the performance of orthogonally sinusoidal flow channels. At 2.0 V, the polarization performances of Case 4-2 and Case 7-2 with the maximum spatial amplitude increase by 15.76% and

16.39%, respectively. Meanwhile, the oxygen content at 40 mm away from the inlet also decreases by 33.87% and 42.63%, respectively. The hydrogen content of Case 5-2 with the maximum horizontal angular frequency increases by 11.07% compared with Case 1-1. However, Case 5-1 and Case 8-1, with the maximum vertical angular frequency, inhibit oxygen removal compared with Case 4-5 and Case 7-5

Nomenclature

BP:	Bipolar plate
CH:	Channel
GDL:	Gas diffusion layer
CL:	Catalytic layer
PEM:	Proton exchange membrane
V_{upper} :	Curve of the upper wall in the left view
V_{lower} :	Curve of the lower wall in the left view
H_{left} :	Curve of the left wall in the top view
H_{right} :	Curve of the right wall in the top view
H :	The difference between the curve equations of the right and left walls
V :	The difference between the curve equations of the upper and lower
S :	The sinusoidal curve of the walls projected
\hat{S} :	The sinusoidal curve of opposite frequency
L :	The linear curve of the walls projected
$i_{v,a}$:	Anode local electrochemical reaction rate
$i_{v,c}$:	Cathode local electrochemical reaction rate
$i_{0,a}$:	Anode reference exchange current density (A/m^2)
$i_{0,c}$:	Cathode reference exchange current density (A/m^2)
α_a :	Anode charge transfer coefficient
α_c :	Cathode charge transfer coefficient
η_a :	Anode activation overpotential (V)
η_c :	Cathode activation overpotential (V)
$\varepsilon_{\text{GDL}}^p$:	GDL porosity
$\varepsilon_{\text{CL}}^p$:	CL porosity
κ_{GDL} :	GDL permeability (m^2)
κ_{CL} :	CL permeability (m^2)
φ_s :	Solid overpotential (V)
φ_m :	Electrolyte overpotential (V)
E_{eq} :	Equilibrium potential (V)
$E_{\text{eq,ref}}(T)$:	Temperature-dependent value of reversible cell voltage (V)
T :	Temperature (K)
σ_s :	Electron conductivity of the solid phase electrode (S/m)
σ_m :	Proton conductivity of the proton exchange membrane (S/m)
ρ_l :	Liquid water density (kg/m^3)
ρ_g :	Gas density (kg/m^3)
u_l :	Liquid water velocity vector (m/s)
u_g :	Gas velocity vector (m/s)
R :	Universal gas constant (C/mol)
F :	Faraday constant ($J/(mol \cdot K)$)
P :	Pressure (Pa)

ε^p :	Porosity of porous media
I :	Transposition symbol
p_l :	Liquid water pressure (Pa)
p_g :	Gas pressure (Pa)
μ_g :	Dynamic viscosity of gas (Pa·s)
μ_l :	Dynamic viscosity of liquid water (Pa·s)
k :	Thermal conductivity ($W/(m \cdot K)$)
C_p :	Heat capacity ($J/(kg \cdot K)$)
S_l :	Source term of liquid-phase mass conservation ($kg/(m^3 \cdot s)$)
S_g :	Source term of gas-phase mass conservation ($kg/(m^3 \cdot s)$)
S_s :	Source term of solid overpotential (A/m^3)
S_m :	Source term of electrolyte overpotential (A/m^3)
S_T :	Source term of energy equation (W/m^3).

Variables

A_{z_1} :	Amplitudes of the left and right wall curve functions (mm)
A_{z_2} :	Amplitude of the upper wall curve function (mm)
ω_l :	Angular frequency of the left wall curve function (rad/s)
ω_r :	Angular frequency of the right wall curve function (rad/s)
ω_k :	Angular frequency of the upper wall curve function (rad/s).

Subscripts

a :	Anode side
c :	Cathode side
O_2 :	Oxygen
H_2 :	Hydrogen
H_2O :	Water
s :	Solid
m :	Membrane
f :	Fluid
eq :	Equilibrium
eff :	Effective.

Data Availability

The data that support the findings of this study are available from the corresponding author upon reasonable request.

Conflicts of Interest

The authors declare that they have no conflicts of interest.

Acknowledgments

This work is financially supported by the National Key Research and Development Program of China (No. 2022YFB4002100), the Projects for Dalian Youth Star of Science and Technology (2021RQ135), the Fundamental Research Funds for the Central Universities (No. 3132023503), and the open research fund from the state key laboratory of rolling and automation, Northeastern University (No. 2023RALKFKT002).

References

- [1] N. Zheng, H. F. Zhang, L. Q. Duan, and Q. S. Wang, "Comprehensive sustainability assessment of a novel solar-driven PEMEC-SOFC-based combined cooling, heating, power, and storage (CCHPS) system based on life cycle method," *Energy*, vol. 265, p. 126343, 2023.
- [2] K. Sonowal and L. Saikia, "Metal-organic frameworks and their composites for fuel and chemical production via CO₂ conversion and water splitting," *RSC Advances*, vol. 12, no. 19, pp. 11686–11707, 2022.
- [3] X. L. Fang, W. Dong, Y. B. Wang, and Q. Yang, "Multiple time-scale energy management strategy for a hydrogen-based multi-energy microgrid," *Applied Energy*, vol. 328, p. 120195, 2022.
- [4] I. Pavić, N. Čović, and H. Pandžić, "PV-battery-hydrogen plant: cutting green hydrogen costs through multi-market positioning," *Applied Energy*, vol. 328, article 120103, 2022.
- [5] G. Jiang, H. M. Yu, J. K. Hao et al., "An effective oxygen electrode based on Ir_{0.6}Sn_{0.4}O₂ for PEM water electrolyzers," *Journal of Energy Chemistry*, vol. 39, pp. 23–28, 2019.
- [6] Z. Wang, X. Wang, Z. Chen, Z. Liao, C. Xu, and X. Du, "Energy and exergy analysis of a proton exchange membrane water electrolysis system without additional internal cooling," *Renewable Energy*, vol. 180, pp. 1333–1343, 2021.
- [7] H. S. Shin and B. S. Oh, "Water transport according to temperature and current in PEM water electrolyzer," *International Journal of Hydrogen Energy*, vol. 45, no. 1, pp. 56–63, 2020.
- [8] J. L. Young, Z. Kang, F. Ganci, S. Madachy, and G. Bender, "PEM electrolyzer characterization with carbon-based hardware and material sets," *Electrochemistry Communications*, vol. 124, p. 106941, 2021.
- [9] G. Zhao, M. R. Kraglund, H. L. Frandsen et al., "Life cycle assessment of H₂O electrolysis technologies," *International Journal of Hydrogen Energy*, vol. 45, no. 43, pp. 23765–23781, 2020.
- [10] G. Yang, J. Mo, Z. Kang et al., "Additive manufactured bipolar plate for high-efficiency hydrogen production in proton exchange membrane electrolyzer cells," *International Journal of Hydrogen Energy*, vol. 42, no. 21, pp. 14734–14740, 2017.
- [11] Z. Y. Kang, J. K. Mo, G. Q. Yang et al., "Thin film surface modifications of thin/tunable liquid/gas diffusion layers for high-efficiency proton exchange membrane electrolyzer cells," *Applied Energy*, vol. 206, pp. 983–990, 2017.
- [12] J. O. Abe, A. P. I. Popoola, E. Ajenifuja, and O. M. Popoola, "Hydrogen energy, economy and storage: review and recommendation," *International Journal of Hydrogen Energy*, vol. 44, no. 29, pp. 15072–15086, 2019.
- [13] F. M. Nafchi, E. Afshari, and E. Baniasadi, "Anion exchange membrane water electrolysis: numerical modeling and electrochemical performance analysis," *International Journal of Hydrogen Energy*, vol. 52, Part D, pp. 306–321, 2024.
- [14] G. Yang, J. Mo, Z. Kang et al., "Fully printed and integrated electrolyzer cells with additive manufacturing for high-efficiency water splitting," *Applied Energy*, vol. 215, pp. 202–210, 2018.
- [15] B. Yodwong, D. Guilbert, M. Phattanasak, W. Kaewmanee, M. Hinaje, and G. Vitale, "AC-DC converters for electrolyzer applications: state of the art and future challenges," *Electronics*, vol. 9, no. 6, p. 912, 2020.
- [16] R. Yang, J. Yesuraj, and K. Kim, "Effect of flow channel shape and operating temperature on the performance of a proton exchange membrane electrolyzer cell," *Energy Fuels*, vol. 37, no. 16, pp. 12178–12191, 2023.
- [17] Y. Wang, Y. H. Pang, H. Xu, A. Martinez, and K. S. Chen, "PEM fuel cell and electrolysis cell technologies and hydrogen infrastructure development - a review," *Energy & Environmental Science*, vol. 15, no. 6, pp. 2288–2328, 2022.
- [18] J. Nie and Y. Chen, "Numerical modeling of three-dimensional two-phase gas-liquid flow in the flow field plate of a PEM electrolysis cell," *International Journal of Hydrogen Energy*, vol. 35, no. 8, pp. 3183–3197, 2010.
- [19] S. N. Özdemir and I. Taymaz, "Three-dimensional modeling of gas-liquid flow in the anode bipolar plate of a PEM electrolyzer," *Journal of the Brazilian Society of Mechanical Sciences*, vol. 44, no. 8, p. 354, 2022.
- [20] B. Gayen, N. K. Manna, and N. Biswas, "Enhanced mixing quality of ring-type electroosmotic micromixer using baffles," *Chemical Engineering and Processing- Process Intensification*, vol. 189, article 109381, 2023.
- [21] T. Smolinka, E. Ojong, and T. Lickert, "Fundamentals of PEM water electrolysis," in *PEM Electrolysis for Hydrogen Production Principles and Applications*, D. Bessarabov and H. J. Wang, Eds., pp. 11–33, CRC Press LLC, Boca Raton, 2015.
- [22] M. Bilgili, M. Bosomoiu, and G. Tsotridis, "Gas flow field with obstacles for PEM fuel cells at different operating conditions," *International Journal of Hydrogen Energy*, vol. 40, no. 5, pp. 2303–2311, 2015.
- [23] F. N. Khatib, T. Wilberforce, J. Thompson, and A. G. Olabi, "Experimental and analytical study of open pore cellular foam material on the performance of proton exchange membrane electrolyzers," *International Journal of Thermofluids*, vol. 9, article 100068, 2021.
- [24] X. Wang, Z. Wang, Y. Feng et al., "Three-dimensional multi-phase modeling of a proton exchange membrane electrolysis cell with a new interdigitated-jet hole flow field," *Science China Technological Sciences*, vol. 65, no. 5, pp. 1179–1192, 2022.
- [25] G. D. Wang, H. Y. Wang, L. Jiang, P. J. Lin, J. R. Li, and J. C. Sun, "Numerical study on dual-region mass transport at wave flow field of proton exchange membrane fuel cell," *Fuel Cells*, vol. 22, no. 1-2, pp. 12–22, 2022.
- [26] A. Tugirumubano, H. J. Shin, S. H. Go, M. S. Lee, L. K. Kwac, and H. G. Kim, "Electrochemical performance analysis of a PEM water electrolysis with cathode feed mode based on flow passage shape of titanium plates," *International Journal of Precision Engineering and Manufacturing*, vol. 17, no. 8, pp. 1073–1078, 2016.
- [27] S. Toghyani, E. Afshari, E. Baniasadi, and S. A. Atyabi, "Thermal and electrochemical analysis of different flow field patterns in a PEM electrolyzer," *Electrochimica Acta*, vol. 267, pp. 234–245, 2018.
- [28] S. Toghyani, E. Afshari, and E. Baniasadi, "Three-dimensional computational fluid dynamics modeling of proton exchange membrane electrolyzer with new flow field pattern," *Journal of Thermal Analysis and Calorimetry*, vol. 135, no. 3, pp. 1911–1919, 2019.
- [29] Y. Zhou, B. Chen, K. Meng et al., "Optimization and evaluation criteria of water-gas transport performance in wave flow channel for proton exchange membrane fuel cell," *International Journal of Hydrogen Energy*, vol. 48, no. 54, pp. 20717–20733, 2023.
- [30] J. O. Majasan, J. I. S. Cho, I. Dedigama, D. Tsaoulidis, P. Shearing, and D. J. L. Brett, "Two-phase flow behaviour

- and performance of polymer electrolyte membrane electrolysers: electrochemical and optical characterisation,” *International Journal of Hydrogen Energy*, vol. 43, no. 33, pp. 15659–15672, 2018.
- [31] H. Li, H. Nakajima, A. Inada, and K. Ito, “Effect of flow-field pattern and flow configuration on the performance of a polymer-electrolyte-membrane water electrolyzer at high temperature,” *International Journal of Hydrogen Energy*, vol. 43, no. 18, pp. 8600–8610, 2018.
- [32] A. S. Tijani, D. Barr, and A. H. A. Rahim, “Computational modelling of the flow field of an electrolyzer system using CFD,” *Energy Procedia*, vol. 79, pp. 195–203, 2015.
- [33] J. K. Kuo and C. K. Chen, “Evaluating the enhanced performance of a novel wave-like form gas flow channel in the PEMFC using the field synergy principle,” *Journal of Power Sources*, vol. 162, no. 2, pp. 1122–1129, 2006.
- [34] J. K. Kuo, T. H. Yen, and C. K. Chen, “Three-dimensional numerical analysis of PEM fuel cells with straight and wave-like gas flow fields channels,” *Journal of Power Sources*, vol. 177, no. 1, pp. 96–103, 2008.
- [35] Y. Zhou, B. Chen, W. S. Chen, Q. H. Deng, J. Shen, and Z. K. Tu, “A novel opposite sinusoidal wave flow channel for performance enhancement of proton exchange membrane fuel cell,” *Energy*, vol. 261, p. 125383, 2022.
- [36] Z. Wang, C. Xu, X. Wang, Z. Liao, and X. Du, “Numerical investigation of water and temperature distributions in a proton exchange membrane electrolysis cell,” *Science China Technological Sciences*, vol. 64, no. 7, pp. 1555–1566, 2021.
- [37] Z. Zhang and X. Xing, “Simulation and experiment of heat and mass transfer in a proton exchange membrane electrolysis cell,” *International Journal of Hydrogen Energy*, vol. 45, no. 39, pp. 20184–20193, 2020.
- [38] F. Aubras, J. Deseure, J. J. A. Kadjo et al., “Two-dimensional model of low-pressure PEM electrolyser: two-phase flow regime, electrochemical modelling and experimental validation,” *International Journal of Hydrogen Energy*, vol. 42, no. 42, pp. 26203–26216, 2017.
- [39] H. Guo, Q. Guo, F. Ye, C. F. Ma, X. Zhu, and Q. Liao, “Three-dimensional two-phase simulation of a unitized regenerative fuel cell during mode switching from electrolytic cell to fuel cell,” *Energy Conversion and Management*, vol. 195, pp. 989–1003, 2019.
- [40] A. Nouri-Khorasani, E. T. Ojong, T. Smolinka, and D. P. Wilkinson, “Model of oxygen bubbles and performance impact in the porous transport layer of PEM water electrolysis cells,” *International Journal of Hydrogen Energy*, vol. 42, no. 48, pp. 28665–28680, 2017.
- [41] T. F. Cao, H. Lin, L. Chen, Y. L. He, and W. Q. Tao, “Numerical investigation of the coupled water and thermal management in PEM fuel cell,” *Applied Energy*, vol. 112, pp. 1115–1125, 2013.
- [42] A. C. Olesen, C. Rømer, and S. K. Kær, “A numerical study of the gas-liquid, two-phase flow maldistribution in the anode of a high pressure PEM water electrolysis cell,” *International Journal of Hydrogen Energy*, vol. 41, no. 1, pp. 52–68, 2016.
- [43] S. Toghiani, E. Baniasadi, and E. Afshari, “Numerical simulation and exergoeconomic analysis of a high temperature polymer exchange membrane electrolyzer,” *International Journal of Hydrogen Energy*, vol. 44, no. 60, pp. 31731–31744, 2019.
- [44] A. H. Hassan, X. Wang, Z. Liao, and C. Xu, “Numerical investigation on the effects of design parameters and operating conditions on the electrochemical performance of proton exchange membrane water electrolysis,” *Journal of Thermal Science*, vol. 32, no. 6, pp. 1989–2007, 2023.
- [45] F. Marangio, M. Santarelli, and M. Cali, “Theoretical model and experimental analysis of a high pressure PEM water electrolyser for hydrogen production,” *International Journal of Hydrogen Energy*, vol. 34, no. 3, pp. 1143–1158, 2009.
- [46] A. Awasthi, K. Scott, and S. Basu, “Dynamic modeling and simulation of a proton exchange membrane electrolyzer for hydrogen production,” *International Journal of Hydrogen Energy*, vol. 36, no. 22, pp. 14779–14786, 2011.
- [47] D. S. Falcão and A. M. F. R. Pinto, “A review on PEM electrolyzer modelling: guidelines for beginners,” *Journal of Cleaner Production*, vol. 261, article 121184, 2020.
- [48] H. R. Zhou, K. Meng, W. S. Chen, and B. Chen, “3D two-phase and non-isothermal modeling for PEM water electrolyzer: heat and mass transfer characteristic investigation,” *International Journal of Energy Research*, vol. 46, no. 12, pp. 17126–17143, 2022.
- [49] L. C. Xia, C. Z. Zhang, M. H. Hu et al., “Investigation of parameter effects on the performance of high-temperature PEM fuel cell,” *International Journal of Hydrogen Energy*, vol. 43, no. 52, pp. 23441–23449, 2018.
- [50] S. Toghiani, E. Afshari, and E. Baniasadi, “Metal foams as flow distributors in comparison with serpentine and parallel flow fields in proton exchange membrane electrolyzer cells,” *Electrochimica Acta*, vol. 290, pp. 506–519, 2018.
- [51] Y. Chen, F. Mojica, G. Li, and P. Y. A. Chuang, “Experimental study and analytical modeling of an alkaline water electrolysis cell,” *International Journal of Energy Research*, vol. 41, no. 14, pp. 2365–2373, 2017.
- [52] A. Kumar, N. K. Manna, S. Sarkar, and N. Biswas, “Analysis of a square split-and-recombined electroosmotic micromixer with non-aligned inlet-outlet channels,” *Nanoscale and Microscale Thermophysical Engineering*, vol. 27, no. 1, pp. 55–73, 2023.
- [53] F. Y. Yan, X. J. Pei, and J. Yao, “Numerical simulation of performance improvement of PEMFC by four-serpentine wave flow field,” *Ionics*, vol. 29, no. 2, pp. 695–709, 2023.
- [54] K. Amit, A. Datta, N. Biswas, S. Das, and P. Das, “Designing of microsink to maximize the thermal performance and minimize the entropy generation with the role of flow structures,” *International Journal of Heat and Mass Transfer*, vol. 176, article 121421, 2021.
- [55] I. S. Anyanwu, Y. Hou, F. Xi et al., “Comparative analysis of two-phase flow in sinusoidal channel of different geometric configurations with application to PEMFC,” *International Journal of Hydrogen Energy*, vol. 44, no. 26, pp. 13807–13819, 2019.
- [56] L. Ma, S. Sui, and Y. Zhai, “Investigations on high performance proton exchange membrane water electrolyzer,” *International Journal of Hydrogen Energy*, vol. 34, no. 2, pp. 678–684, 2009.
- [57] Y. Sui, C. J. Teo, P. S. Lee, Y. T. Chew, and C. Shu, “Fluid flow and heat transfer in wavy microchannels,” *International Journal of Heat and Mass Transfer*, vol. 53, no. 13–14, pp. 2760–2772, 2010.
- [58] Z. Tian, Z. K. Huang, Y. Zhou, Z. Cao, and W. Z. Gao, “Design and experimental study on wave-type microchannel cooling plates for marine large-capacity battery thermal management,” *Applied Thermal Engineering*, vol. 236, p. 121571, 2024.
- [59] M. Rabiei, A. Gharehghani, and A. M. Andwari, “Enhancement of battery thermal management system using a novel structure of hybrid liquid cold plate,” *Applied Thermal Engineering*, vol. 232, p. 121051, 2023.